Journal of Membrane Science 671 (2023) 121397

Contents lists available at ScienceDirect

Journal of Membrane Science

journal homepage: www.elsevier.com/locate/memsci

Enhanced CO_2/H_2 separation by GO and PVA-GO embedded PVAm nanocomposite membranes

Wenqi Xu [a], Arne Lindbråthen [a], Saravanan Janakiram [b], Luca Ansaloni [b], Liyuan Deng [a,*]

[a] Department of Chemical Engineering, Norwegian University of Science and Technology (NTNU), Trondheim, NO, 7491, Norway
[b] Department of Sustainable Energy Technology, SINTEF Industry, 0373, Oslo, Norway

ARTICLE INFO

Keywords:
Graphene oxide
Facilitated transport
Nanocomposite membrane
CO_2 separation
H_2 purification

ABSTRACT

Membrane technology for CO_2/H_2 separation, especially when using CO_2-selective membranes to keep H_2 on the high-pressure retentate side, has been considered promising and energy-efficient for further H_2 transport and utilization. This work prepared and optimized a CO_2-selective membrane based on polyvinylamine (PVAm) with embedded graphene oxide (GO) and grafted GO for CO_2/H_2 separation. The facilitated transport effect of PVAm enhances CO_2 transport, while the GO-based 2D nanosheets bring in a barrier effect to compensate for the high H_2 diffusivity. The GO-modified surface with higher CO_2 affinity also provides additional CO_2 sorption sites. The membranes' chemical structure, thermal stability, and morphology were characterized. The effects of GO and PVA-GO in the PVAm matrix and optimal loadings of GO or PVA-GO were investigated. Introducing GO into PVAm significantly increased CO_2 permeance with a slight increase in CO_2/H_2 selectivity. While by adding 0.5 wt % PVA-GO, CO_2/H_2 selectivity significantly increased from 10 to 22. The selective layer thickness also greatly affects CO_2/H_2 separation. By increasing the coating layer thickness to approx. 11 μm, the CO_2/H_2 selectivity substantially increased. The separation performances of the studied membrane are far above the current CO_2/H_2 upper bound.

1. Introduction

The increasing level of atmospheric CO_2 is directly linked to global warming and the rising sea level [1]. Carbon capture, utilization, and storage (CCUS) are well accepted as the most effective way to reduce CO_2 emissions over the following decades. In CCUS, CO_2 capture is mainly from power generation through two pathways: post-combustion and pre-combustion. The post-combustion process needs to treat a mixture of CO_2 and N_2 in the flue gas with low CO_2 concentration and low CO_2 partial pressure. On the other hand, pre-combustion is the conversion of fossil fuel to H_2 (syngas) or enabling different green sources of H_2 (such as biohydrogen) as the fuel before combustion, which always includes a CO_2/H_2 separation step to separate H_2 from a mixture saturated with water and containing CO_2. H_2 has a high calorific value, and the product of H_2 combustion is water, thus avoiding dust, CO_2 emissions, and other contaminant gases encountered in post-combustion for power generation [2,3]. Therefore, efficient removal of CO_2 from H_2-containing sources, such as syngas and bio-hydrogen from dark-fermentation, is critical to enabling H_2 as a fuel, reducing CO_2 emissions, and ensuring the safety of H_2 transportation and utilization. It is worth mentioning that in syngas separation, CO_2 concentration (approx. 35%) and CO_2 partial pressure are high, which means a high driving force for the separation [4,5], while for bio-H_2 separation from bioreactors, the separation conditions are milder with much lower CO_2 partial pressure at ambient temperature.

Nowadays, the technologies used in industry for separating CO_2 and H_2 are mainly pressure swing adsorption (PSA), cryogenic distillation, chemical absorption, and physical absorption [6,7]. In recent decades, the use of membranes for CO_2 and H_2 separation has become a promising alternative to current methods due to its low energy consumption, small footprint, low capital and operating cost, operational simplicity, and few chemical additives [8,9]. However, no CO_2/H_2 separation membranes have been applied in industrial process as yet mainly due to the lack of membranes with sufficient CO_2/H_2 selectivity. Recently, Ho and co-workers reported excellent performances of CO_2/H_2 failitated transport membranes at high temperatures (>100 °C) with a thickness of ≥17 μm [10–14]. Nevertheless, the reported membranes are in favor of high temperature to promote the CO_2 transport by mobile carriers, thus were not yet developed for separation at moderated conditions for bio-hydrogen separation.

* Corresponding author.
E-mail address: liyuan.deng@ntnu.no (L. Deng).

https://doi.org/10.1016/j.memsci.2023.121397
Received 28 November 2022; Received in revised form 3 January 2023; Accepted 15 January 2023
Available online 18 January 2023

Another approach to improve CO_2/H_2 selectivity is to introduce 2-dimensional (2D) nanosheets into a polymeric facilitated transport membrane matrix with well aligned nanostructure in the nanocomposite coating layer. A schematic illustration of a nanocomposite membrane with a selective layer containing 2D nanosheets on a porous substrate is shown in Fig. 1.

Addition of nanofillers into a polymeric matrix for fabrication of the selective layer is a tried and tested approach to enhance gas separation and overcome the "trade-off" between selectivity and permeability in membranes, known as "upper bounds" [15–17]. The most studied polymeric membranes for CO_2/H_2 separation are H_2-selective membranes governed by the solution-diffusion mechanism, which up-concentrates H_2 at the low pressure permeate side while keeping CO_2 on the retentate side (high-pressure side). However, it is beneficial if H_2 is retained at the high-pressure side to save recompression energy in H_2 transport and utilization, i.e., by using CO_2-selective membranes. However, polymeric membranes based on solution-diffusion usually show relatively low CO_2/H_2 separation performances largely due to the smaller molecular size of H_2 (2.89 Å) than CO_2 (3.3 Å) and hence much higher H_2 diffusivity [8,9]. Applying facilitated transport mechanism can effectively change the membrane separation from H_2-selective to CO_2-selective. An illustration of how CO_2 transports through a CO_2-selective facilitated transport membrane is shown in Fig. 2.

Facilitated transport membranes may involve two classes of carriers: fixed site carriers (FSC) and mobile carriers (Fig. 2). Fixed site carriers are CO_2-reactive functional groups that are attached to polymer backbones (e.g., amino groups in PVAm or poly(allylamine) (PAAm)), while mobile carriers are small CO_2-reactive organic compounds with mobility, such as amino acid salts and alkanolamines [18,19]. The reversible reaction in the FSC membrane matrix can be described by a zwitterion mechanism, as presented in Eq. (1) [20]. It must be mentioned that when water is present, the reversible reaction involving water actively contributes to the facilitated transport effect in facilitated transport, as shown in Eq. (2) [21,22]. Thus, when facilitated transport is applied in membrane separation, water is no longer an impurity, unlike in most solution-diffusion membranes [23], but becomes an important promotor for the separation.

$$2RNH_2 + CO_2 \Longleftrightarrow 2RNHCOO^- + 2RNH_3^+ \quad (1)$$

$$2CO_2 + 2RNH_2 + H_2O \Longleftrightarrow RHNCOOH + HCO_3^- + RNH_3^+ \quad (2)$$

Ideally, more amino groups can provide higher CO_2/H_2 selectivity. Of all polymers, PVAm has the highest content of amino groups directly attached to its backbone [24]. Therefore, PVAm has been widely used in fixed carrier facilitated transport membranes and is selected as the basic membrane material for CO_2/H_2 separation in this work.

The main challenge for CO_2/H_2 separation using PVAm membrane is that despite exceeding the CO_2/H_2 upper bound, the CO_2/H_2 selectivity is still not sufficient to attract industrial applications [25,26]. Adding nanofillers to prepare nanocomposite membranes with nanofillers properties is expected to further improve the gas separation properties [15,17,27]. In this work, incorporating 2D nanofillers, especially graphene oxide (GO)-based, within PVAm facilitated membranes is expected to be able to increase the CO_2/H_2 selectivity. This approach to improve CO_2/H_2 separation performance has rarely been reported.

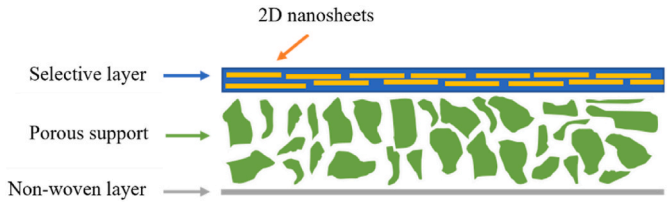

Fig. 1. Nanocomposite membrane with embedded 2D nanosheets in the selective layer on a porous substrate.

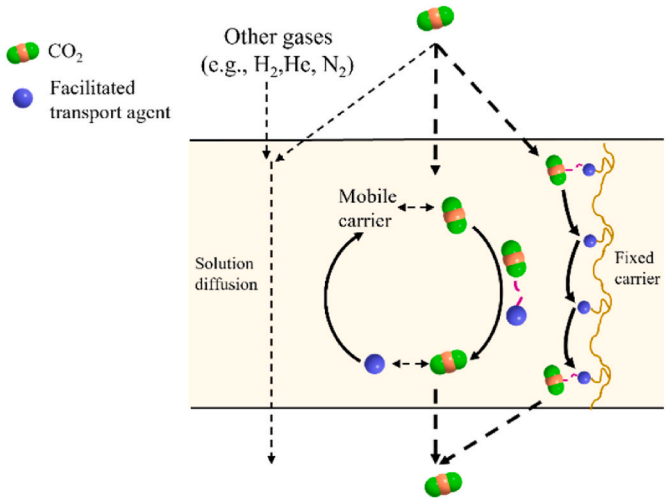

Fig. 2. CO_2 transport through a CO_2-selective facilitated transport membrane.

Due to the high aspect ratio for barrier properties, 2D nanosheets such as GO should be good candidates as nanofiller to influence gas separation performances [28]. Based on literature study [29–31], following hypothesis on the addition of GO-based nanosheets are proposed: *i)* for CO_2/H_2 separation, GO nanosheets are impermeable to gases, increasing gas separation selectivity against smaller molecules; *ii)* the presence of oxygen-containing groups, for instance, epoxy, hydroxyl, and carbonyl of GO have interfacial interactions with CO_2 to enhance preferential permeation properties, such as increased CO_2 sorption capacity; and *iii)* presence of nanosheets orientates the polymer chain packing, leading to higher specific free volume [32]. A key challenge in incorporating 2D nanofillers is often the poor compatibility of nanofillers with the polymer matrix, which can lead to the formation of voids between the nanofillers and the matrix, resulting in the loss of selectivity. Grafting GO with additives (e.g., polyvinyl alcohol (PVA)) containing matrix-affinity groups can improve the compatibility of the GO nanosheets because the grafted polymer chains wrap and/or cover part of GO surface, making it in "polymer-to-polymer" contact interface. PVA is a hydrogel and shows good compatibility with PVAm [22,33,34]. The hydroxyl in the PVA forms strong interfacial interactions (hydrogen bonds) with the oxygen-containing groups of GO. Therefore, PVA is used as the grafting additive of GO in this study. Wu et al. reported using poly (2,3-epoxy-1-propanol) (PEP) as a grafting additive to almost double CO_2/H_2 selectivity [35]. Janakiram et al. prepared poly (ethylene glycol)-grafted-GO/SHPAA/PVA membranes for CO_2/N_2 separation, resulted in a CO_2/N_2 selectivity increase of approx. 38% compared with the GO/SHPAA/PVA [36]. However, few studies have reported grafted GO in membranes for CO_2/H_2 separation.

This work aims to develop a CO_2-selective membrane based on the facilitated transport mechanism with high CO_2/H_2 selectivity. GO-based 2D nanosheets were introduced to further improve the separation. GO and PVA grafted GO (PVA-GO) were embedded in the PVAm matrix to prepare nanocomposite membranes with different contents of GO and PVA-GO, and the membranes were optimized for enhanced CO_2/H_2 separation. Membranes and membrane materials were characterized to evaluate their physical, chemical, and separation properties using SEM, FTIR, TGA, and gas permeation tests and optimized accordingly. The gas separation permeances of the membranes were measured under fully humidified conditions. The effects of the selective layer thickness of membranes were also studied. Incorporating GO or PVA-GO with PVAm enhanced CO_2/H_2 gas separation performance.

2. Materials and methods

2.1. Materials

Lupamin® 9095 was received from BASF AG Germany. Polyvinyl alcohol (PVA, Mw:85,000–124,000, 87–89% hydrolyzed), sodium hydroxide (NaOH, 97%) and hydrochloric acid (HCl, 37%) were purchased from Sigma-Aldrich, Norway. Acetone (≥98%), and ethanol absolute (EtOH) were purchased from VWR, Norway. Graphene oxide (GO, <100 mesh) was kindly donated by LayerOne, Norway. Two types of polysulfone ultrafiltration (UF) membranes (GR51PP and GR40PP) were purchased from Alfa Laval Nordic AS with the molecular weight cut-off (MWCO) of 50k and 20k, respectively. Polyethersulfone UF membranes (PES, 30k MWCO and 50k MWCO) and polyvinylidene fluoride (PVDF, 30k MWCO) UF membranes were provided by Synder Filtration, USA. The epoxy glue Loctite 3430 was purchased from TOOLS, Norway, and the Avery Dennison 180 aluminum foils used to seal the membranes were received from Norsk Filmtrykk AS. CO_2/He gas mixture (10 vol% CO_2 in He) used for the permeation test was received from Linde Gas AS, Norway.

2.2. Purification of PVAm solution

Lupamin® 9095 contains a high concentration of salt, which will have a negative influence on membrane gas separation performances. Thus, multiple purification procedures were applied to ensure a good performance and homogeneous membranes matrix, part of which can be found in the literature [12,37,38]. For the readers' convenience, a brief description is given as follows: Lupamin® 9095 was precipitated by dropping it into an acetone/EtOH mixture with stirring. The precipitation was filtrated, washed, and dried in a vacuum oven. It was repeated several times until purified PVAm was obtained. Finally, 3.0 wt% PVAm solution was prepared with the pH value adjusted to 10 using a 5 M NaOH solution.

2.3. Preparation of GO solution

The GO solution preparation follows the main procedure reported by Janakiram et al. [19] with modifications to suit the specific circumstances of this work. GO particle as received was dissolved into DI water to prepare 1 mg/g GO solution. 5 M NaOH was added to adjust the pH of the diluted solution to 10. The solution was sonicated in a sonification bath with ice for 30 min. The dispersed solution was sonicated again in ultrasonic disintegration (Vibra-Cell™ Ultrasonic Liquid Processor) at an amplitude of 60% in an ice bath, with a 3-s pulse, 2-s break, and 6 h of operation time to ensure exfoliation and a thorough dispersion.

2.4. Synthesis of PVA-GO

The procedure of PVA-GO synthesis is described by Kashyap et al. [39] and can be briefly outlined as follows: 7g PVA was dissolved in 93 mL DI water at 95 °C with refluxing until dissolving completely. A certain amount of dispersed GO solution (GO concentration: 0.75 wt% of PVA) was dropwise added to the PVA solution under vigorous stirring to obtain a homogeneous solution. Subsequently, the solution was vigorously stirred under 60 °C. Finally, a very fine brown-to-black and high viscosity PVA-GO solution, including 0.034 wt% GO and 0.046 wt% PVA, was obtained. The proposed structure scheme of PVA-GO is illustrated in Fig. 3.

2.5. Preparation of membranes

All membranes were coated using dip coating. A certain amount (0.25 wt%, 0.5 wt%, 0.75 wt% and 1.0 wt%) of GO and PVAm was mixed into four different solutions, and all the PVAm/GO sample solutions were sonicated in the sonification bath for 3 min. The total solid concentration was diluted to 1.5%. The GO content (ω_{GO}, wt.%) in all the membranes was calculated by Eq. (3):

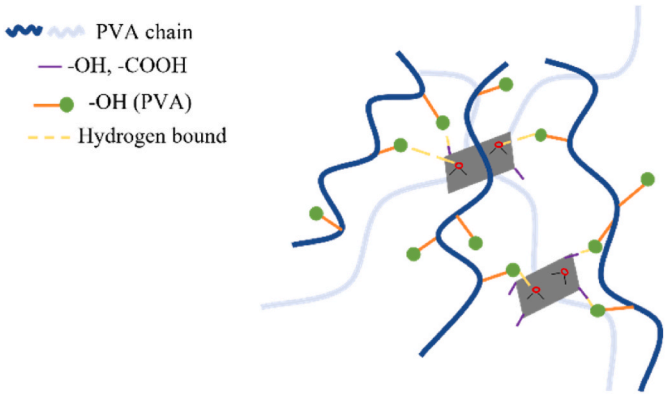

Fig. 3. Conceptual sketch of PVA-GO structure. The light blue lines represent the PVA chains attached to the backside of the GO sheets. (For interpretation of the references to colour in this figure legend, the reader is referred to the Web version of this article.)

$$\omega_{GO} = \frac{m_{GO}}{m_{GO} + m_{PVAm}} \times 100\% \quad (3)$$

where m_{PVAm} is the weight of PVAm and m_{GO} is the weight of GO.

After the preparation of PVA-GO, the concentration of GO and PVA was measured as 0.034 wt% and 0.046 wt% in the PVA-GO solution, respectively. Thus, in order to keep the same GO content in the membrane matrix, the PVA-GO content (ω_{PVA-GO}, wt.%) in all the membranes was calculated by Eq. (4):

$$\omega_{PVA-GO} = \frac{m_{GO}}{\frac{m_{GO}}{0.034\ \%} + m_{PVAm}} \times 100\% \quad (4)$$

In order to find an optimal substrate membrane, PVAm solution was coated on to five different commercial UF membranes to compare their performance. PSF (50k and 20k), PES (30k and 50k) and PVDF (30k) were used as the support membranes, and the 3.0 wt% PVAm was coated onto these supports using a dip coating machine (KCV NIMA, Biolin Scientific, Finland) under identical conditions. Firstly, all the support membranes were washed with warm tap water for 1 h (~45 °C) and later with DI water for at least half an hour. Then, the mounted membranes were coated by dip-coating with the PVAm solution (membrane soaking for 30 s) and dried in air for approx. 8h. After that, the coated membranes were turned upside-down for a second coating following the same procedure. The prepared membranes were then dried at 40 °C under 800 mbar vacuum overnight to ensure that the membranes were completely dry. Before testing, membranes were treated at 90 °C in a ventilated oven for 1h to induce physical cross-linking. After the optimal support was determined, all membranes in this work followed the same procedure described here. The prepared membranes are presented as PVAm/GO-X and PVAm/(PVA-GO)-X where X (0.25, 0.5, 0.75, and 1) in the study are denoted as the mass percentage of GO or PVA-GO relative to the total solid concentration. Membranes with different thicknesses were also coated following the same procedure, but with a varying number of coating dips, for example, 2 times, 4 times, and 12 times (flipping direction between alternative dips). For membrane material characterizations, dry materials were used after drying samples at 45 °C under approx. 280 mbar.

Fig. 4 summarizes the brief procedure of membrane preparation and testing in this work. All membranes reported in this paper were prepared following the same procedure. At least three membranes of the same composition were tested for the reported performances.

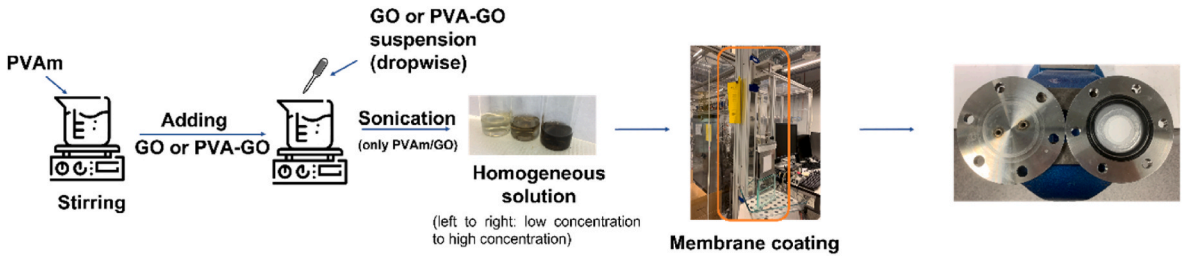

Fig. 4. A brief presentation of membrane preparation and testing procedure.

2.6. Characterization of materials and membranes

Fourier-transform infrared (FT-IR) spectrometer (Thermo Nicolet Nexus) was used to provide information on chemical bonds inside the dry samples. FT-IR spectra of PVAm, GO, PVA-GO, PVAm/GO-X, and PVAm/PVA-GO-X were measured within the scan range between 800 and 4000 cm^{-1}.

The weight loss during heat treatment was determined using thermogravimetric analysis (TGA, Thermal Scientific Q500). The TGA experiments were performed in a nitrogen atmosphere. Heating routes were based on heat treatment procedures with different materials or membranes, and the heating rate was set at 5 °C/min. The purge and cooling gas is nitrogen, with a flow rate of 20 mL/min.

The viscosity of PVA-GO solution was measured by rheological tests performed using the Thermal Scientific HR-2. The investigated solutions were placed in the 1 mm gap between parallel plates ($D_y = 40$ mm), and the shear speed was set from 1 s^{-1} to 100 s^{-1} under room temperature.

A contact angle goniometer (Attension Theta, Biolin Scientific) was used to measure the contact angle between support and membrane solution, and coated selective layer and membrane solution (after 2-, 4-, 6-, 8-, 10-, and 12-time coating). A liquid drop with a volume of 3–5 μL was used, and the contact angle reported in the paper was calculated by the average between opposing initial contact angles.

The surface and cross-sectional morphology of the membranes were studied using Field Emission Scanning Microscope (FE-SEM, ZEISS Supra-55 VP, manufactured by Carl Zeiss NTS GmbH, Germany). Before analysis, membranes were cryogenically fractured in liquid nitrogen to get cross-sectional figures, and membranes were sputtered with a thin layer of gold to enhance conductivity.

2.7. Mixed-gas separation experiments

The mixed gas performance of nanocomposite membranes was tested using a home-made apparatus as reported in Ref. [40] and shown in Fig. 5.

Gas mixtures of CO_2/He (10 vol% CO_2/90 vol% He) and CO_2/H_2 (10 vol% CO_2/90 vol% H_2) were used as the feed gas under 1.7 bar, while in this work, N_2 was introduced as the sweep gas at the permeate side to adjust the CO_2 partial pressure for the lab-scale testing (at approx. 1.05 bar) instead of applying vacuum pressures. All the tests are at 25 °C and kept under ~100% relative humidity in both feed gas and sweep gas streams. A membrane module with an effective area of approx. 6 cm^2 was used. The flow rate of feed gas and sweep gas was measured by two mass flow controllers. The concentrations of CO_2 and He from the sweep side were measured by a calibrated gas chromatograph (490 Micro GC, Agilent). After reaching the steady state, the permeance of CO_2 ($\frac{P_i}{l}$) can be obtained by Eq. (5):

$$\frac{P_i}{l} = \frac{N_{perm}\left(1 - y_{H_2O}\right)y_i}{A\left(p_{i,feed} - p_{i,perm}\right)} \tag{5}$$

where P_i is the permeability of CO_2 and N_{perm} is the total permeate flow rate that was measured by using a bubble flow meter, y_{H_2O} is the mole fraction of water in the permeate flow calculated according to the relative humidity and the vapor pressure according to the testing condition, y_i is the molar fraction gas specie i in the permeate side, A is the effective membrane area, and $p_{i,feed}$ and $p_{i,perm}$ is the partial pressure of gas specie i in the feed and permeate side, respectively.

The gas separation factor (selectivity of gas pair in the engineering field) was determined by mole fractions between two different gas species as in Eq. (6):

$$\alpha_{i/j} = \frac{y_i/y_j}{x_i/x_j} \tag{6}$$

where y_i and y_j are the mole fractions of gas species i and j in the permeate side, and x_i and x_j are the mole fractions of gas species i and j in the feed side.

It is worth noting that, due to strict safety requirements in our laboratory, CO_2/He gas mixture was used instead of CO_2/H_2 during the membrane material optimization stage in this work. The optimal ratio was then measured using CO_2/H_2 to test the gas separation performance. It is considered a common practice because Helium has the closest molecular size to H_2 and is a very safe gas to work with [41,42]. A selected membrane was tested for CO_2/H_2 separation to compare with CO_2/He separation performance and verify this method, thereby limiting the number of experiments with H_2. A CO_2/H_2 (10 vol% CO_2/90 vol% H_2) was used to measure the neat PVAm membrane under the same testing conditions. The subsequently obtained He permeance was 2.22 ± 0.48 GPU, and H_2 permeance was 2.37 ± 0.72 GPU. As the difference between He permeance and H_2 permeance is only ~6%, lower than 10% (the acceptable deviation for experimental data in this work), it is reasonable to use CO_2/He separation performances as the indication for membrane optimization for CO_2/H_2 separation.

PVAm membranes with different UF membranes as porous supports were compared with regard to their CO_2/He separation performance to select the optimal substrate. At least three membranes with different loadings of GO or PVA-GO were tested to ensure stabilized performance and data reproducibility; the standard deviation of all performance data is controlled. The average values from the tests were used for each set of reported performance data. All the gas separation performance data

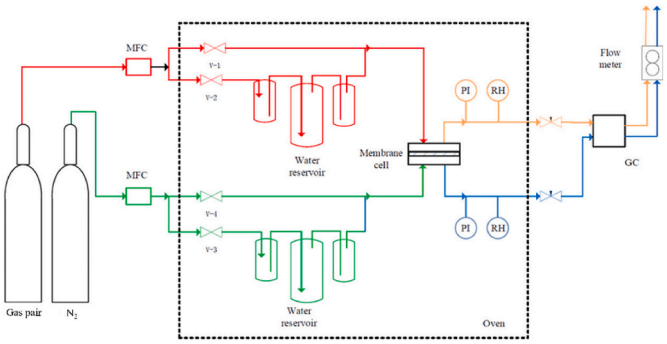

Fig. 5. Humid mixed gas permeation testing rig. MFC: mass flow controller; PI: pressure indicator; RH: relative humidity sensor and GC: gas chromatography. Reproduced from Ref. [40].

reported in this work were obtained with a standard deviation lower than 10% except specially mentioned in this paper; Thus, the error bars were not presented.

3. Results and discussions

3.1. Chemical structure analysis of PVAm/GO and PVAm/PVA-GO nanocomposites

The FT-IR analysis was used to investigate the interaction between PVAm and GO or PVA-GO and their interaction difference due to PVA-GO grafting, as shown in Fig. 6.

A comparison of PVAm and PVAm/GO-X is displayed in Fig. 6 (a). A broad peak and a small but clear peak can be observed for all samples in the higher energy region from 3400 cm^{-1} to 2740 cm^{-1}, which is associated with C–NH_2 and C–H stretching vibrations of PVAm [43]. Sharp peaks are positioned between 1750 cm^{-1} and 1500 cm^{-1} because of C═O and C═C stretching vibration, which are the representative peaks of GO [44]. Two clear and prominent peaks can be detected between 1250 cm^{-1} and 1000 cm^{-1} of PVAm/GO, which are assigned to C–O stretching and C–*O*–C stretching vibrations associated to GO [45].

Compared with the peaks of PVAm/GO-X in Fig. 6 (A), peaks at 1750 cm^{-1} and 1500 cm^{-1} (C═O carboxylic acid groups and C═C stretching of PVA-GO, respectively) for PVAm/(PVA-GO)-X, as presented in Fig. 6 (b), have slightly shifted of the wavenumber than that of PVAm/GO samples [46]. The peak at 3300 cm^{-1} of PVAm/PVA-GO is much wider than PVAm/GO, which is attributed to the intermolecular hydrogen bonds in the polymer and in the low wavelength range, and there is a new peak at 835 $cm^{-1,}$ which might be = C–H bending [39]. Thus, shifted or widened peaks and appearing new peaks are strong evidence that GO has already been grafted by PVA [46].

3.2. Thermal properties of GO and PVA-GO in PVAm

TGA was used to exam the thermal properties of all the membrane materials, and the results are presented in Fig. 7.

From Fig. 7 (a) and (b), it is clear that at the low temperature range (≤100 °C), a small amount of weight loss is observed due to water loss. The mass losses in the second stage, in the range of 110–475 °C, are characteristic of PVAm/GO and PVAm/PVA-GO. The curves show the degradation of PVAm with onset temperature (T_{onset}) of 190–220 C°, and during the first degradation of the polymer, ammonia and hydrazine bonds are broken [47]. Between 220 and 475 C°, the most labile functional groups, oxygen-containing functional groups, decompose. Above 475 C°, the thermal decomposition of the carbon backbone of PVAm and GO occur. Due to using N_2 as inert gas, the remaining weight is the carbon that cannot be removed from the system. Adding GO and PVA-GO does not have a significant influence on the decomposition temperature of PVAm except for the case of PVAm/(PVA-GO)-1. Incorporating 1.0 wt% PVA-GO into PVAm shows a totally different trend in the TGA curve. Compared with other loadings, the PVAm/(PVA-GO)-1 shows higher stability even until approx. 250 °C. This might be because the high loading of PVA/GO acts as an IR/thermal-shield which can protect the polymer chains from being subjected to heat [48], and it may also indicate the altered structure of PVAm polymer matrix due to the good compatibility of the polymer and PVA-GO nanofillers as well as the strong influence of the larger amount of PVA-GO than the optimal loading.

Fig. 7 (c) shows the TGA curve of GO and PVA-GO, and it can be used to roughly calculate the content of grafted PVA on GO. The calculation method was reported by Cheng et al. [46]. The weight loss for GO at 1000 °C was about 66.81 wt%. Before 100 °C, PVA-GO has a slight weight loss (2.95 wt%) due to water loss, which is included in the calculation. For the PVA-GO, the weight loss is approx. 92.0 wt%. According to these results, there are around 25 wt% PVA and 75 wt% GO in the PVA-GO. Therefore, it can be confirmed that part of the GO surfaces has been grafted by PVA.

3.3. Membrane morphology

FE-SEM has been used to investigate the morphology of membranes. Fig. 8 presents the FE-SEM images of the PVAm/GO membranes. According to the FE-SEM images from different part of the coated flat sheet membranes, a defect-free selective layer has been successfully coated onto the porous support. No obvious pore filling was observed. Theoretically, the coating thickness of membranes should be similar if the concentration and viscosity of the coating solution are similar. However, PVAm/(PVA-GO)-0.5 membrane exhibits a higher thickness of the selective layer than that of the PVAm/GO-0.5, which is believed to be due to the relatively high viscosity of the PVA-GO solution (0.037 Pa s). Further increasing PVA-GO concentration, the thickness of the selective layer increases. Both PVAm/GO-0.5 and PVAm/(PVA-GO)-0.5 membranes show a smooth surface. However, in the PVAm/(PVA-GO)-1.0 membranes, aggregation spots were observed on the surface, possibly because of the poor dispersion of PVA-GO under high GO concentration in solutions with relatively high viscosity.

3.4. Mixed gas permeation study

3.4.1. Selection of porous supports

In order to find the most suitable porous support in this work, membranes coated with the same polymer solution (3.0 wt% PVAm) on

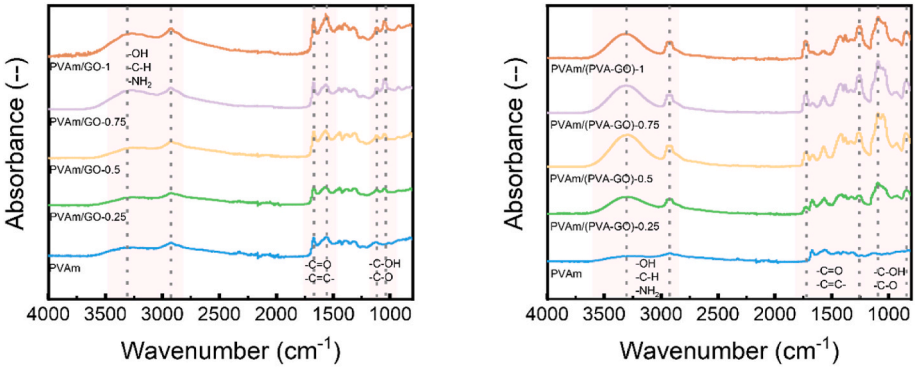

Fig. 6. FT-IR spectra of (a) PVAm and PVAm/GO-X; (b) PVAm and PVAm/PVA-GO-X.

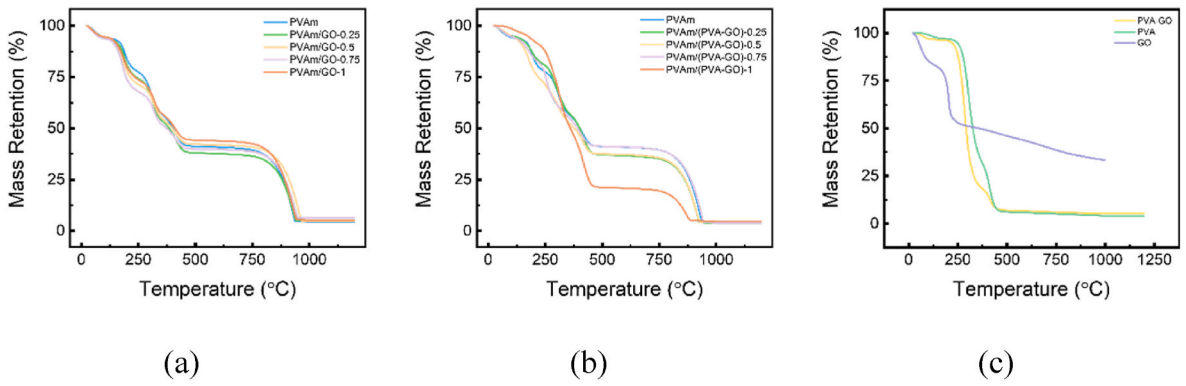

Fig. 7. TGA curves of PVAm and PVAm/GO-X (a) and PVAm and PVAm/PVA-GO-X (b), and PVA-GO and GO (c).

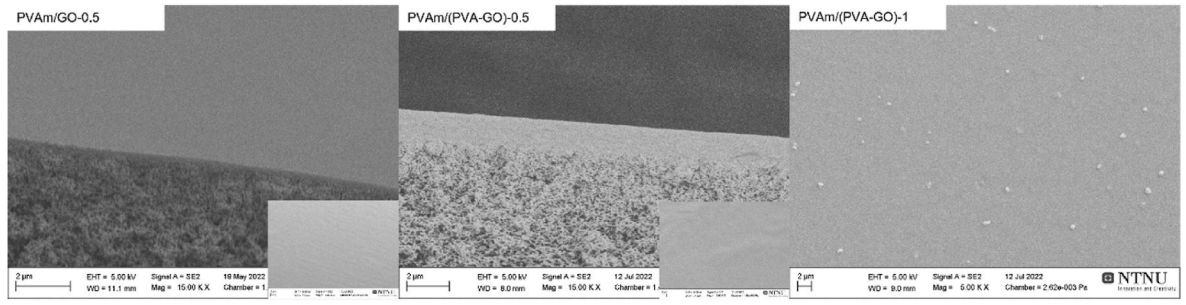

Fig. 8. Cross-section and surface (inset) SEM images of PVAm/GO-0.5 (a), PVAm/(PVA-GO)-0.5 (b), and the surface of PVAm/(PVA-GO)-1 (c).

five different commercially available UF membranes were tested using the humid mixed gas permeation test rig (Fig. 5), and their performances were compared. According to the literature, the five selected UF membranes (PSf 50k and 20k, PES30k, PES50k, and PVDF30k) are considered the most commonly used substrates to prepare FSC composite membranes. Fig. 9 presents the separation performance of the membranes based on different support substrates.

As it can be seen, among the 5 supports, the two PSf membranes performed better with PVAm membranes. PSf (50k) obtains the highest CO_2 permeance of 84.1 GPU with a low CO_2/He selectivity, while PSf (20k) shows the highest CO_2/He selectivity of 11 with a relatively low CO_2 permeance. Since our main goal has been to improve the selectivity of CO_2 over H_2, PSf (20k) was selected as the porous support and used to prepare all the nanocomposite membranes throughout this study.

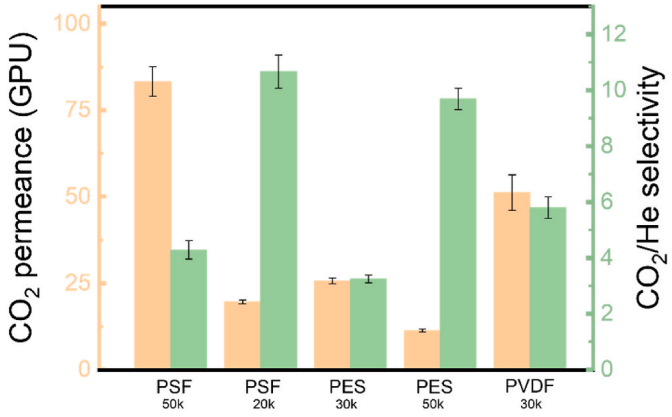

Fig. 9. Comparison of membrane performances of five different support membranes. All membranes were coated with 3.0 wt% PVAm solution on porous supports under the same testing conditions. Tested at 25 °C with a feed pressure of 1.7 bar and ~100% relative humidity.

3.4.2. *Effect of GO loading*

In CO_2-selective facilitated transport membranes, CO_2 transports across the membrane matrix through a reversible reactive pathway in addition to the solution-diffusion transport [32,49], leading to relatively high CO_2/He selectivity. In this work, the facilitated transport effect in the PVAm/GO membranes is brought about by the amino groups of PVAm, which can reversibly react with CO_2 in the presence of water. Due to this facilitated transport effect, the separation performance of neat PVAm membranes reached a CO_2/He selectivity of as high as 11 and CO_2 permeance of ~20 GPU, as presented in Fig. 10, in the absence of GO.

Among other options, 2D GO was selected as nanofillers to enhance

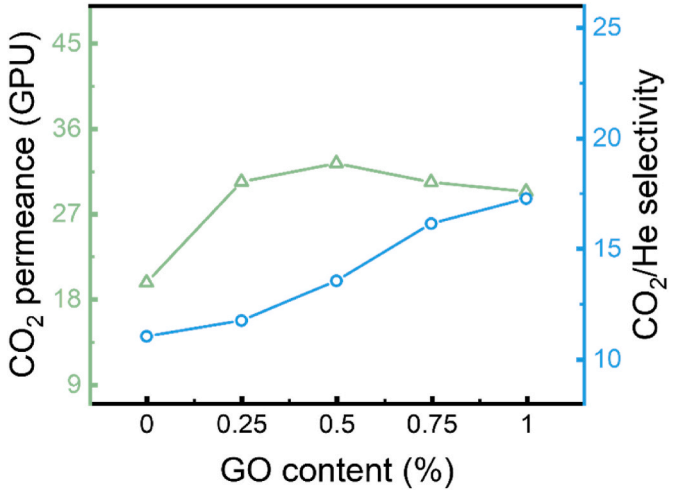

Fig. 10. CO_2/He separation performance of neat PVAm (GO content = 0%) and PVAm/GO membranes of various GO contents. Tested at 25 °C with a feed pressure of 1.7 bar and ~100% relative humidity.

PVAm membranes' performance primarily due to their barrier effect stemming from their high aspect ratio. Thus, the GO-based nanocomposite membranes are expected to decrease gas diffusion, especially towards the faster transport of small molecules such as H_2 and He [50]. In the meanwhile, the large specific surface area of GO introduces a large number of CO_2 sorption sites in the PVAm matrix and, hence, increases the CO_2 solubility in the PVAm/GO nanocomposite [51]. Incorporating GO into PVAm matrix can also induce the reorientation of the polymer chain packing, leading to spatial distribution in the polymer [52], which, together with the fact that the PVAm polymer-GO interface is highly hydrophilic and water is expected to redistribute along the GO surface in the PVAm matrix [53], results in a significant increase in CO_2 permeation according to the strong water involvement in reversible reactions in the facilitated transport, as given by Eq. (2). Last but not least, the mechanical strength and durability of water-swollen membranes under fully humidified conditions are expected to be positively affected by adding GO, thanks to GO's extraordinary mechanical strength [53].

The separation performances of PVAm/GO nanocomposite membranes with different GO contents are presented in Fig. 10. At only a small GO loading of 0.25 wt%, the membrane already shows a sharp increase in CO_2 permeance (from 19.7 to 30.4 GPU, an approx. 54% increment), which to an extent reflects the hypotheses we proposed above, i.e., the embedded GO effectively disrupted the polymer chain packing with rearranged water distribution in the PVAm matrix and brought in additional CO_2 sorption sites, while blocking the smaller molecules from fast diffusion. However, increasing the GO loading from 0.25 wt% to 1.0 wt% did not show further improvement in CO_2 permeance; the CO_2 permeance remains nearly unchanged, or the changes are within the error range. It is believed to be due to the competition between the GO's barrier effect on gas diffusion and the enhancement of CO_2 sorption. Nevertheless, compared with the neat PVAm membrane, CO_2/He selectivity gradually increases with increasing GO loading, and at 1.0% GO loading, the highest CO_2/He selectivity of 17 was obtained, which is approx. 57% higher than that of the neat PVAm membrane. This trend, i.e., increasing selectivity and constant or slightly decreased gas permeance with increasing GO contents, confirms that the barrier effect towards smaller molecules is more significant. According to the literature [36,54] the CO_2 permeation may be further increased by improving the interface contact between GO and the polymer matrix.

3.4.3. *Effect of PVA-GO loading*

In order to further improve the separation performance of the PVAm/GO membranes, GO was grafted with PVA to enhance the compatibility between PVAm and GO. The PVA-GO was then introduced to the PVAm matrix instead of GO. The modified GO may enhance the interfacial interaction between GO and the PVAm matrix, occupy more space around GO, and reduce the formation of voids, but it may also lead to increasing compactness in the interfaces and hence the more barrier effect of GO towards small molecules, which is possible to result in an increase in CO_2/He selectivity.

Fig. 11 shows the CO_2/He separation performance of PVAm/PVA-GO membranes of various PVA-GO contents. Compared with a neat PVAm membrane, adding a tiny amount of PVA-GO (0.25 wt %) to PVAm membrane increases CO_2 separation performance notably with 116% increment in CO_2 permeance (42.5 GPU) and 55% increase in the CO_2/He selectivity (17) (Region I). Increasing the PVA-GO loading to 0.5 wt% further increases the CO_2/He selectivity to 22, but the CO_2 permeance starts to drop (27.8 GPU) (Region II). When the PVA-GO loading increase to 0.75 wt %, both CO_2/He selectivity and CO_2 permeance start to decrease (Region III). Further increase the PVA-GO loading to 1.0 wt %, CO_2/He selectivity significantly decreases to 15, but it is still higher than that of neat PVAm; also, the CO_2 permeance slightly increases (Region IV).

This trend may be explained as follows: *i)* at a relative low loading (region I), due to the interactions between –OH groups of the GO surface and PVAm, more occupied space around GO and between GO and PVAm enhances the barrier property, combating the diffusion of the smaller molecules (He). Introducing PVA-GO into polymeric matrix also introduces more CO_2 sorption sites, leading to higher CO_2 permeation; Thus, both CO_2 permeance and CO_2/He selectivity increase significantly. *ii)* further increase in PVA-GO loading (Region II) continues to increase the CO_2 sorption sites, and the increased tortuous pathways further retards the faster diffusion molecules, leading to enhanced CO_2/He selectivity. However, the increased barrier effect also causes the drop of all gas permeance; *iii)* increasing PVA-GO loading to a relative high range (region III), the barrier effect becomes more dominating. The presence of more PVA-GO nanosheets causes more barriers in the gas transport pathway, hence decreasing the permeance of both CO_2 and He. Moreover, the strong interaction and more compact interface of the GO surface with the PVAm matrix makes the CO_2 carriers (-NH_2) around the GO less accessible, thus the CO_2 facilitated transport becomes less significant, causing the drop in CO_2/He selectivity. Most importantly, according to Yoo et al. [55], the compacted interfaces in this case also lead to the decrease of local water uptake capacity along the GO surface, which somewhat hinders the water transport into the membrane matrix. Thus, the compacted interfaces and their consequent "barrier effect" towards water transport make the water less accessible and CO_2 facilitated transport less effective [22]; *iv)* further increasing PVA-GO loading (region IV), the dispersion of GO may become less efficient and voids may appear, e.g., due to aggregation of GOs. In the meanwhile, all gas permeances, especially of small molecules such as He and H_2, start to increase, which may be attributed to the formation of voids between the nanosheet-polymer interface owing to loadings beyond critical threshold when a larger amount of fillers is embedded. Therefore, the CO_2/He selectivity decreases and CO_2 peremeance increases in this region.

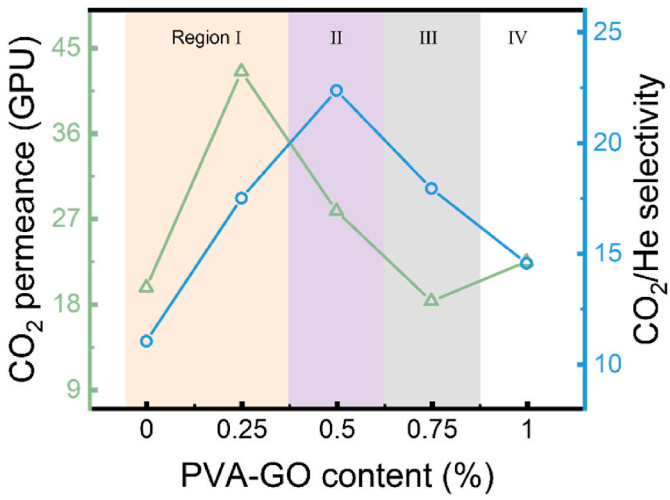

Fig. 11. CO_2/He separation performance of PVAm/PVA-GO membranes of various PVA-GO contents. Tested at 25 °C with a feed pressure of 1.7 bar and ~100% relative humidity.

For an enhanced CO_2/He selectivity, the optimal loading of PVA-GO should be 0.5 wt% based on the performance trend. At this ratio, the CO_2 facilitated transport effect counteracts with the extra resistance caused by additional tortuosity of the impermeable PVA-GO in the membrane [36].

3.4.4. *Effect of selective layer thickness*

As a feature of facilitated transport membranes, membrane thicknesses exhibit substantial influence on membrane separation performance, as explained by the complex transport mechanisms in the membrane matrix, e.g., facilitated transport (reversible reaction) and solution-diffusion transport [56]. The facilitation factor, defined as the

ratio of the overall solute flux to that of based on solution-diffusion, represents the contribution of facilitated transport (reaction between CO_2 and amine groups). It has been reported that performances of PVAm-based membranes are thickness-dependent [12,22]. Therefore, the thickness effect of the nanocomposite membranes was investigated to examine the transport mechanism and find the optimal membrane thickness for CO_2/H_2 separation.

In this work, the thicknesses of selective layers were adjusted by changing the coating times (keeping the same concentration of coating solution) to ensure a defect-free and uniform coating. Theoretically, the coating layer thickness can be estimated. Increasing the coating solution concentration or coating times should increase the thickness of the selective layer linearly, as shown in (7) [57]:

$$h_\infty = \frac{2}{3}\sqrt{\frac{\mu u}{\rho g}} \bullet N \bullet c_p \tag{7}$$

where h_∞ is the thickness of the resulting selective layer, μ is the viscosity of the coating solution, u is withdrawal velocity, ρ is the density of the coating solution, N is coating times, c_p is the concentration of the coating solution, and g is the gravitational acceleration.

As the dispersion of 2D fillers is usually sensitive and prone to aggregation, in this work, the dispersion conditions for GO-based nanofillers in PVAm solutions was opimized and the total solid content in the solution, c_p, was fixed to the optimal amount (1.5 wt%) to avoid aggregation in the membranes and mitigate the uncertainty. Therefore, the thicknesses of the membranes were adjusted only by applying various coating times.

According to the SEM images (Fig. 12 a-f), the thickness of the selective layer increases by increasing the number of coating times as expected. However, the increment of the thickness exhibited two different trends. Firstly, after 2 times of coating, a selective layer thickness of 1.8 μm was obtained on the membrane. When coating 4 times and 6 times of the same solution, only a minor increase in the thickness was observed; the thickness was 2.0 μm and 2.2 μm, respectively. Surprisingly, as shown in Fig. 13 (a), further increasing the coating times brought in significant increase in the thickness, and the increment is proportional with respect to the coating times: the thickness increased from 2.2 μm to 11 μm by coating 6 to 12 times. The different interaction of the membrane solution with the substrates was indicated by measuring contact angles between the membrane solution with the neat support as well as the coated layers (after 2-, 4-, 6-, 8-, 10-, and 12-time coating) as presented in Fig. 13 (b). As it can be seen, 2-time coating and 4-time coating shows similar contact angles (32° and 34.9°, respectively). However, after 6-time coating, the contact angle between the selective layer and membrane solution increases significantly (from 54.1° to ~72°). Further increasing the coating times, the contact angle of that after 8-, 10-, and 12-time coating are nearly unchanged (71.5°, 74°, and 72.63°, respectively). Based on the contact angle values, it is reasonable to assume that when the coating thickness is low, the thickness increment of the coating layer was influenced more prominently by the surface properties of the substrate [58], limiting the growth in the thickness. However, when the distance is large enough with a relatively high thickness (e.g., >2.2 μm), the effect from the substrate surface becomes negligible since the coating layer is now deposited on the surface of the same material with the same charges [58]. Thus, increasing coating time can remarkably increase the coating layer thickness nearly proportionally, as shown in Fig. 13 (a).

Fig. 14 shows the effect of the membrane selective layer thickness on the CO_2/He separation performance, i.e., the selectivity and CO_2 permeability. As expected, with increasing selective layer thickness, the CO_2 permeance decreases but the CO_2 permeability increases. CO_2/He selectivity increase with the thickness as well. When the thickness of the selective layer increases from 1.8 μm to 11 μm, the CO_2 permeance decreases from 27.8 to 15.2 GPU (approx. 46% lower than that of 1.8 μm), but the CO_2 permeability increases from 47.2 to 167 Barrer (approx. 254% higher than that of 1.8 μm), and CO_2/He selectivity increased from 22 to 40 (approx. 82% higher than that of 1.8 μm). Please note that the permeability values were calculated using the selective layer thickness and ignoring the support substrate's transport resistance. When the selective layer is thick enough, the influence of support may be negligible as the porous support contribute little to the overall resistance. But the substrate layer may, to various extents, cause deviation in the permeability value when the selective layer is thin, and the transport resistance of the substrate becomes more significant.

The monotonously increasing CO_2 permeability and the overall increment of the CO_2/He selectivity, along with increasing selective layer thickness, agree well with the characteristic of the facilitated transport mechanism concerning the thickness [56]. The thickness-dependent CO_2 permeability indicates that CO_2 transport in this membrane depends mainly on the CO_2-carrier reaction rate and the diffusion of the CO_2-carrier complex [12]. The solution-diffusion of CO_2 molecules contributes only a minor part of the total CO_2 transport

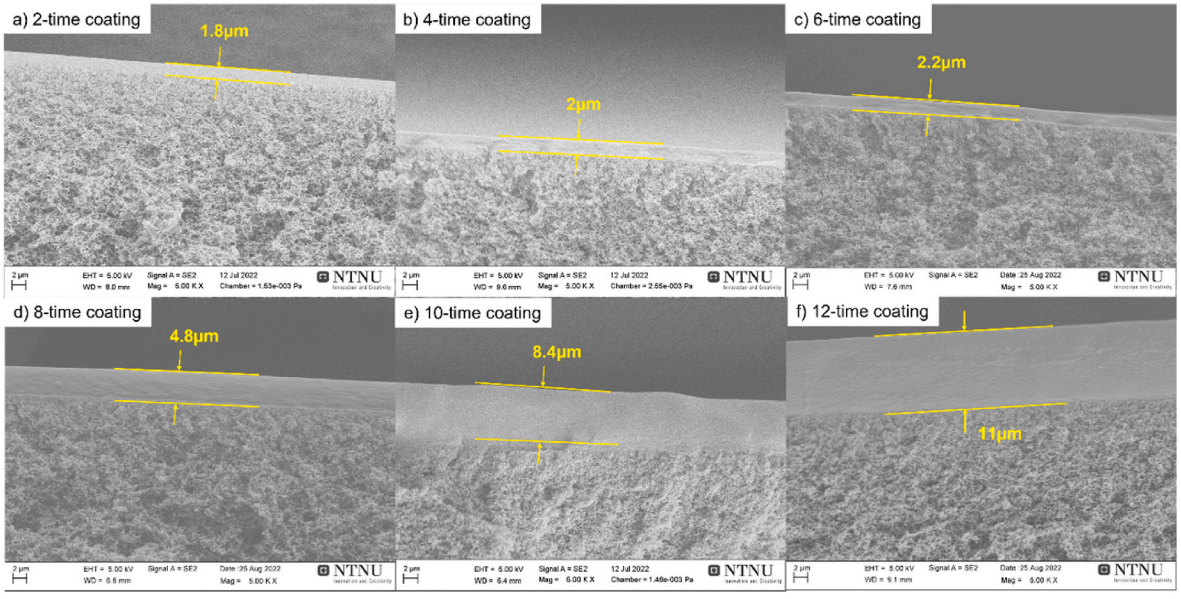

Fig. 12. Cross-section SEM images of membranes by 6 different coating times (a–f).

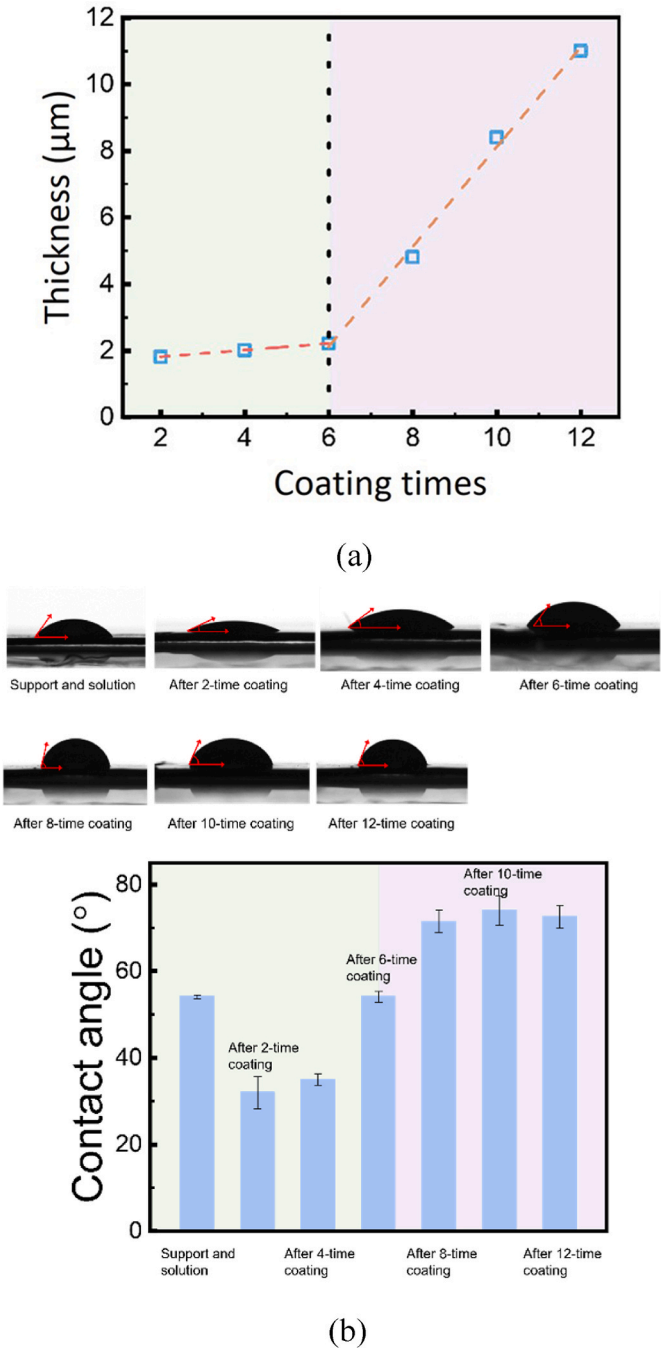

Fig. 13. (a) Selective layer thicknesses of different coating times being influenced (green region) and not influenced (purple region) by the substrate surface; (b) Contact angles of the membrane solution on the PSf supports without and with coating layers. (For interpretation of the references to colour in this figure legend, the reader is referred to the Web version of this article.)

through the membrane as in solution–diffusion governed membranes; the gas permeability should be independent of the membrane thickness. Furthermore, the increasing CO_2/He selectivity with increasing thickness indicates that He transport is not significantly affected by the thickness, which is in line with the solution-diffusion transport of He through the membranes. This tendency is the same as previously reported [33,59,60].

In order to better understand the overall separation performances of the prepared CO_2-selective nanocomposite membranes containing GO or PVA-GO, the experimental data obtained from this work were plotted against the upper bound for CO_2/H_2 separation at 25 °C, where the

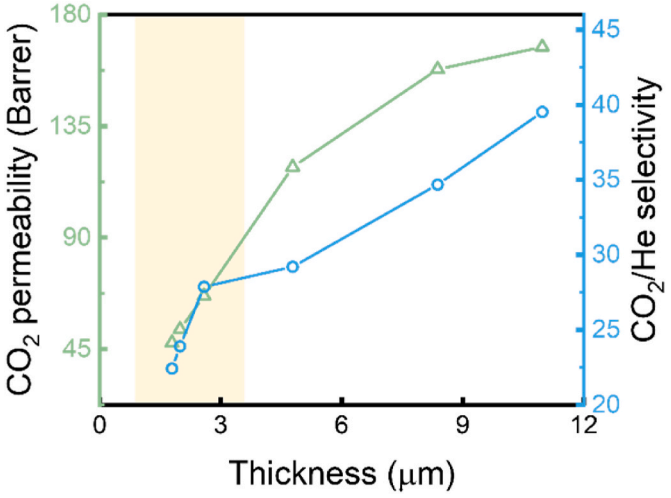

Fig. 14. Effect of selective layer thickness of PVAm/PVA-GO membranes on gas separation performance.

selectivity (separation factor) for each membrane is presented as a function of the CO_2 permeability [16,61]. It is worth mentioning that the permeability data for this work were calculated by ignoring the resistance in the porous substrate, so the actual permeability data for the selective layer material should be even higher.

As presented in Fig. 15, the developed membranes in this work exhibit CO_2/H_2 (CO_2/He) separation performance over the upper bound, and it is clear that the CO_2 permeability and selectivity of CO_2 over H_2 can be simultaneously improved. The PVA-GO/PVAm nanocomposite membrane with a thickness of 11 μm shows the highest CO_2/H_2 selectivity of 22 and CO_2 permeability 61.6 Barrer, which is among the best-performed membranes under similar testing conditions for CO_2/H_2 separation reported in the literature although higher gas separation performances have been reported under much higher temperature and much thicker membranes [10–14]. Further increasing the selective layer thickness may achieve even higher selectivity and CO_2 permeability, but the permeance value will be too low to fulfill the

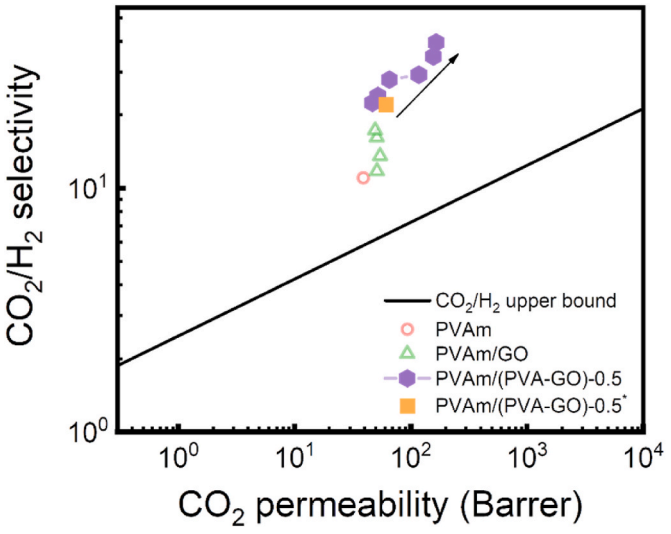

Fig. 15. CO_2/He gas separation performance of neat PVAm, PVAm/GO, and different thickness of PVAm/(PVA-GO)-0.5 in comparison with the CO_2/H_2 upper bound [16,61]. The arrow indicates increasing selective layer thickness. *The yellow square presents the CO_2/H_2 performance by testing the same membrane of the purple hexagons (11 μm as the selective layer thickness). (For interpretation of the references to colour in this figure legend, the reader is referred to the Web version of this article.)

industrialization requirement, thus not tested.

4. Conclusions

CO_2-selective nanocomposite facilitated transport membranes with a PVAm-based selective layer containing 2D nanofillers (GO and PVA-GO) were fabricated and tested with respect to the CO_2/H_2 separation. The effects of adding GO-based nanofillers were investigated by studying the effects of the loadings of two GO-based 2D nanofillers on the CO_2 separation performance. The presence of even a small amount of GO nanosheets benefits CO_2 facilitated transport and significantly increases CO_2/H_2 selectivity. The PVA grafted GO in PVAm leads to a more compact interface due to hydrogen bonding between the amino groups of PVAm matrix with PVA, increasing resistance of both CO_2 and H_2 diffusion, which, consequently, decreases the CO_2 permeance but increases the CO_2/H_2 selectivity, even at a relatively low PVA-GO loading. The performance of the membranes is found to be thickness dependent, and increasing membrane thickness benefits CO_2 transport, showing a typical facilitated transport effect. This membrane with an 11 μm thick selective layer shows CO_2/H_2 selectivity and CO_2 permeability of 22 and 61.6 Barrer, respectively.

The fabricated membranes outperform most reported membranes in the literature for the tested temperature range. In future work, the studied membranes will be tested under relatively high temperatures to investigate the temperature effects on the membrane performance, since the membrane performance may further increase at higher temperatures due to the temperature-dependent CO_2-amine reaction kinetics [62–64] at higher temperatures over 90 °C.

Author statement

Wenqi Xu:
Methodology, Formal analysis, Validation, Investigation, Writing - original draft, Visualization.
Arne Lindbråthen:
Writing - review & editing.
Saravanan Janakiram:
Writing - review & editing.
Luca Ansaloni:
Writing - review & editing, Funding acquisition.
Liyuan Deng:
Conceptualization, Writing - review & editing, Supervision, Project administration, Funding acquisition.
All authors have read and agreed to the published version of the manuscript.

Declaration of competing interest

The authors declare that they have no known competing financial interests or personal relationships that could have appeared to influence the work reported in this paper.

Data availability

Data will be made available on request.

Acknowledgements

This work is a part of the FaT H2 project supported by the Research Council of Norway (No. 294533).

References

[1] E.D. Cartwright, Code red"—recent IPCC report warns time is running out on climate change, Climate and Energy (2021) 11–12.
[2] J.O. Abe, A.P.I. Popoola, E. Ajenifuja, O.M. Popoola, Hydrogen energy, economy and storage: review and recommendation, Int. J. Hydrogen Energy 44 (29) (2019) 15072–15086, https://doi.org/10.1016/j.ijhydene.2019.04.068.
[3] M. İlbaş, S. Karyeyen, A numerical study on combustion behaviours of hydrogen-enriched low calorific value coal gases, Int. J. Hydrogen Energy 40 (44) (2015) 15218–15226, https://doi.org/10.1016/j.ijhydene.2015.04.141.
[4] G. Varvoutis, A. Lampropoulos, E. Mandela, M. Konsolakis, G.E. Marnellos, Recent advances on CO2 mitigation technologies: on the role of hydrogenation route via green H2, Energies 15 (13) (2022) 4790, https://doi.org/10.3390/en15134790.
[5] X. He, D. Chen, Z. Liang, F. Yang, Insight and comparison of energy-efficient membrane processes for CO2 capture from flue gases in power plant and energy-intensive industry, Carbon Capture Science & Technology 2 (2022), 100020, https://doi.org/10.1016/j.ccst.2021.100020.
[6] M. Bui, C.S. Adjiman, A. Bardow, E.J. Anthony, A. Boston, S. Brown, P.S. Fennell, S. Fuss, A. Galindo, L.A. Hackett, J.P. Hallett, H.J. Herzog, G. Jackson, J. Kemper, S. Krevor, G.C. Maitland, M. Matuszewski, I.S. Metcalfe, C. Petit, G. Puxty, J. Reimer, D.M. Reiner, E.S. Rubin, S.A. Scott, N. Shah, B. Smit, J.P.M. Trusler, P. Webley, J. Wilcox, N. Mac Dowell, Carbon capture and storage (CCS): the way forward, Energy Environ. Sci. 11 (5) (2018) 1062–1176, https://doi.org/10.1039/c7ee02342a.
[7] W.Y. Hong, A Techno-Economic Review on Carbon Capture, Utilisation and Storage Systems for Achieving a Net-Zero CO2 Emissions Future, Carbon Capture Science & Technology, 2022, 100044, https://doi.org/10.1016/j.ccst.2022.100044.
[8] Y. Han, W.S.W. Ho, Recent advances in polymeric facilitated transport membranes for carbon dioxide separation and hydrogen purification, J. Polym. Sci. 58 (18) (2020) 2435–2449, https://doi.org/10.1002/pol.20200187.
[9] M. Czyperek, P. Zapp, H.J.M. Bouwmeester, M. Modigell, K. Ebert, I. Voigt, W. A. Meulenberg, L. Singheiser, D. Stover, Gas separation membranes for zero-emission fossil power plants: MEM-BRAIN, J. Membr. Sci. 359 (1–2) (2010) 149–159, https://doi.org/10.1016/j.memsci.2010.04.012.
[10] Y. Yang, Y. Han, R. Pang, W.S.W. Ho, Amine-containing membranes with functionalized multi-walled carbon nanotubes for CO2/H2 separation, Membranes 10 (11) (2020) 333, https://doi.org/10.3390/membranes10110333.
[11] Y. Zhao, B.T. Jung, L. Ansaloni, W.W. Ho, Multiwalled carbon nanotube mixed matrix membranes containing amines for high pressure CO2/H2 separation, J. Membr. Sci. 459 (2014) 233–243.
[12] L. Ansaloni, Y.N. Zhao, B.T. Jung, K. Ramasubramanian, M.G. Baschetti, W.S. W. Ho, Facilitated transport membranes containing amino-functionalized multi-walled carbon nanotubes for high-pressure CO2 separations, J. Membr. Sci. 490 (2015) 18–28, https://doi.org/10.1016/j.memsci.2015.03.097.
[13] Y.N. Zhao, W.S.W. Ho, Steric hindrance effect on amine demonstrated in solid polymer membranes for CO2 transport, J. Membr. Sci. 415 (2012) 132–138, https://doi.org/10.1016/j.memsci.2012.04.044.
[14] Z. Tong, W.S.W. Ho, New sterically hindered polyvinylamine membranes for CO2 separation and capture, J. Membr. Sci. 543 (2017) 202–211, https://doi.org/10.1016/j.memsci.2017.08.057.
[15] S. Janakiram, M. Ahmadi, Z. Dai, L. Ansaloni, L. Deng, Performance of nanocomposite membranes containing 0D to 2D nanofillers for CO2 separation: a review, Membranes 8 (2) (2018) 24, https://doi.org/10.3390/membranes8020024.
[16] L.M. Robeson, The upper bound revisited, J. Membr. Sci. 320 (1–2) (2008) 390–400, https://doi.org/10.1016/j.memsci.2008.04.030.
[17] M. Ahmadi, S. Janakiram, Z.D. Dai, L. Ansaloni, L.Y. Deng, Performance of mixed matrix membranes containing porous two-dimensional (2D) and three-dimensional (3D) fillers for CO2 separation: a review, Membranes 8 (3) (2018) 50, https://doi.org/10.3390/membranes8030050.
[18] Z. Tong, W.S.W. Ho, Facilitated transport membranes for CO2 separation and capture, Separ. Sci. Technol. 52 (2) (2017) 156–167, https://doi.org/10.1080/01496395.2016.1217885.
[19] S. Janakiram, J.L.M. Espejo, K.K. Hoisaeter, A. Lindbrathen, L. Ansaloni, L.Y. Deng, Three-phase hybrid facilitated transport hollow fiber membranes for enhanced CO2 separation, Appl. Mater. Today 21 (2020), 100801, https://doi.org/10.1016/j.apmt.2020.100801.
[20] M. Caplow, Kinetics of carbamate formation and breakdown, J. Am. Chem. Soc. 90 (24) (1968) 6795–6803, https://doi.org/10.1021/ja01026a041.
[21] G. Sartori, W. Ho, D. Savage, G. Chludzinski, S. Wlechert, Sterically-hindered amines for acid-gas absorption, Separ. Purif. Methods 16 (2) (1987) 171–200, https://doi.org/10.1080/03602548708058543.
[22] L.Y. Deng, T.J. Kim, M.B. Hagg, Facilitated transport of CO2 in novel PVAm/PVA blend membrane, J. Membr. Sci. 340 (1–2) (2009) 154–163, https://doi.org/10.1016/j.memsci.2009.05.019.
[23] M. Saeed, S. Rafiq, L.H. Bergersen, L.Y. Deng, Tailoring of water swollen PVA membrane for hosting carriers in CO2 facilitated transport membranes, Separ. Purif. Technol. 179 (2017) 550–560, https://doi.org/10.1016/j.seppur.2017.02.022.
[24] R. Pelton, Polyvinylamine: a tool for engineering interfaces, Langmuir 30 (51) (2014) 15373–15382, https://doi.org/10.1021/la5017214.
[25] Z. Qiao, Z. Wang, S. Yuan, J. Wang, S. Wang, Preparation and characterization of small molecular amine modified PVAm membranes for CO2/H2 separation, J. Membr. Sci. 475 (2015) 290–302, https://doi.org/10.1016/j.memsci.2014.10.034.
[26] X.C. Cao, H.Q. Xu, S.L. Dong, J.Y. Xu, Z.H. Qiao, S. Zhao, J.X. Wang, Z. Wang, Preparation of high-performance and pressure-resistant mixed matrix membranes for CO2/H-2 separation by modifying COF surfaces with the groups or segments of

the polymer matrix, J. Membr. Sci. 601 (2020), 117882, https://doi.org/10.1016/j.memsci.2020.117882.
[27] L. Ansaloni, L. Deng, Advances in polymer-inorganic hybrids as membrane materials, recent developments in polymer macro, Micro and nano blends, Elsevier, 163-206, https://doi.org/10.1016/B978-0-08-100408-1.00007-8, 2017.
[28] H.B. Park, J. Kamcev, L.M. Robeson, M. Elimelech, B.D. Freeman, Maximizing the right stuff: the trade-off between membrane permeability and selectivity, Science 356 (6343) (2017), https://doi.org/10.1126/science.aab0530 eaab0530.
[29] J.S. Bunch, S.S. Verbridge, J.S. Alden, A.M. van der Zande, J.M. Parpia, H. G. Craighead, P.L. McEuen, Impermeable atomic membranes from graphene sheets, Nano Lett. 8 (8) (2008) 2458–2462, https://doi.org/10.1021/nl801457b.
[30] H.W. Kim, H.W. Yoon, S.M. Yoon, B.M. Yoo, B.K. Ahn, Y.H. Cho, H.J. Shin, H. Yang, U. Paik, S. Kwon, J.Y. Choi, H.B. Park, Selective gas transport through few-layered graphene and graphene oxide membranes, Science 342 (6154) (2013) 91–95, https://doi.org/10.1126/science.1236098.
[31] Z.P. Smith, B.D. Freeman, Graphene oxide: a new platform for high-performance gas- and liquid-separation membranes, Angew Chem. Int. Ed. Engl. 53 (39) (2014) 10286–10288, https://doi.org/10.1002/anie.201404407.
[32] D.D. Peng, S.F. Wang, Z.Z. Tian, X.Y. Wu, Y.Z. Wu, H. Wu, Q.P. Xin, J.F. Chen, X. Z. Cao, Z.Y. Jiang, Facilitated transport membranes by incorporating graphene nanosheets with high zinc ion loading for enhanced CO2 separation, J. Membr. Sci. 522 (2017) 351–362, https://doi.org/10.1016/j.memsci.2016.09.040.
[33] L.Y. Deng, M.B. Hagg, Carbon nanotube reinforced PVAm/PVA blend FSC nanocomposite membrane for CO2/CH4 separation, Int. J. Greenh. Gas Control 26 (2014) 127–134, https://doi.org/10.1016/j.ijggc.2014.04.018.
[34] L.Y. Deng, M.B. Hagg, Fabrication and evaluation of a blend facilitated transport membrane for CO2/CH4 separation, Ind. Eng. Chem. Res. 54 (44) (2015) 11139–11150, https://doi.org/10.1021/acs.iecr.5b02971.
[35] Y. Wu, P. Jia, L. Xu, Z. Chen, L. Xiao, J. Sun, J. Zhang, Y. Huang, C.W. Bielawski, J. Geng, Tuning the surface properties of graphene oxide by surface-initiated polymerization of epoxides: an efficient method for enhancing gas separation, ACS Appl. Mater. Interfaces 9 (5) (2017) 4998–5005, https://doi.org/10.1021/acsami.6b14895.
[36] S. Janakiram, J.L.M. Espejo, X.Y. Yu, L. Ansaloni, L.Y. Deng, Facilitated transport membranes containing graphene oxide-based nanoplatelets for CO2 separation: effect of 2D filler properties, J. Membr. Sci. 616 (2020), 118626, https://doi.org/10.1016/j.memsci.2020.118626.
[37] Y.X. Chen, W.S.W. Ho, High-molecular-weight polyvinylamine/piperazine glycinate membranes for CO2 capture from flue gas, J. Membr. Sci. 514 (2016) 376–384, https://doi.org/10.1016/j.memsci.2016.05.005.
[38] T.J. Kim, H. Vralstad, M. Sandru, M.B. Hagg, Separation performance of PVAm composite membrane for CO2 capture at various pH levels, J. Membr. Sci. 428 (2013) 218–224, https://doi.org/10.1016/j.memsci.2012.10.009.
[39] S. Kashyap, S.K. Pratihar, S.K. Behera, Strong and ductile graphene oxide reinforced PVA nanocomposites, J. Alloys Compd. 684 (2016) 254–260, https://doi.org/10.1016/j.jallcom.2016.05.162.
[40] Z. Dai, J. Deng, Q. Yu, R.M.L. Helberg, S. Janakiram, L. Ansaloni, L. Deng, Fabrication and evaluation of bio-based nanocomposite TFC hollow fiber membranes for enhanced CO2 capture, ACS Appl. Mater. Interfaces 11 (11) (2019) 10874–10882, https://doi.org/10.1021/acsami.8b19651.
[41] Z.D. Dai, L. Ansaloni, L.Y. Deng, Precombustion CO2 capture in polymeric hollow fiber membrane contactors using ionic liquids: porous membrane versus nonporous composite membrane, Ind. Eng. Chem. Res. 55 (20) (2016) 5983–5992, https://doi.org/10.1021/acs.iecr.6b01247.
[42] J. Ilconich, C. Myers, H. Pennline, D. Luebke, Experimental investigation of the permeability and selectivity of supported ionic liquid membranes for CO2/He separation at temperatures up to 125 degrees C, J. Membr. Sci. 298 (1–2) (2007) 41–47, https://doi.org/10.1016/j.memsci.2007.03.056.
[43] Y.X. Qiu, T.H. Zhang, M. Ruegsegger, R.E. Marchant, Novel nonionic oligosaccharide surfactant polymers derived from poly(vinylamine) with pendant dextran and hexanoyl groups, Macromolecules 31 (1) (1998) 165–171, https://doi.org/10.1021/ma9707401.
[44] M. Mirza-Aghayan, M. Heidarian, M. Mohammadi, R. Boukherroub, Synthesis and characterization of a novel multi-functionalized reduced graphene oxide as a pH-sensitive drug delivery material and a photothermal candidate, Appl. Surf. Sci. (2022), 152568, https://doi.org/10.1016/j.apsusc.2022.152568.
[45] L. Chen, Z.W. Xu, J.L. Li, B.M. Zhou, M.J. Shan, Y.L. Li, L.S. Liu, B.D. Li, J.R. Niu, Modifying graphite oxide nanostructures in various media by high-energy irradiation, RSC Adv. 4 (2) (2014) 1025–1031, https://doi.org/10.1039/c3ra46203j.
[46] H.K. Cheng, N.G. Sahoo, Y.P. Tan, Y. Pan, H. Bao, L. Li, S.H. Chan, J. Zhao, Poly (vinyl alcohol) nanocomposites filled with poly(vinyl alcohol)-grafted graphene oxide, ACS Appl. Mater. Interfaces 4 (5) (2012) 2387–2394, https://doi.org/10.1021/am300550n.
[47] R. Casadei, D. Venturi, M. Giacinti Baschetti, L. Giorgini, E. Maccaferri, S. Ligi, Polyvinylamine membranes containing graphene-based nanofillers for carbon capture applications, Membranes 9 (9) (2019) 119, https://doi.org/10.3390/membranes9090119.
[48] M. Mazurkiewicz-Pawlicka, M. Nowak, A. Malolepszy, A. Witowski, D. Wasik, Y. Hu, L. Stobinski, Graphene oxide with controlled content of oxygen groups as a filler for polymer composites used for infrared radiation shielding, Nanomaterials 10 (1) (2019) 32, https://doi.org/10.3390/nano10010032.
[49] J. Huang, J. Zou, W.S.W. Ho, Carbon dioxide capture using a CO2-selective facilitated transport membrane, Ind. Eng. Chem. Res. 47 (4) (2008) 1261–1267, https://doi.org/10.1021/ie070794r.
[50] J. Shen, G. Liu, K. Huang, W. Jin, K.R. Lee, N. Xu, Membranes with fast and selective gas-transport channels of laminar graphene oxide for efficient CO2 capture, Angew Chem. Int. Ed. Engl. 54 (2) (2015) 578–582, https://doi.org/10.1002/anie.201409563.
[51] A. Ali, R. Pothu, S.H. Siyal, S. Phulpoto, M. Sajjad, K.H. Thebo, Graphene-based membranes for CO2 separation, Materials Science for Energy Technologies 2 (1) (2019) 83–88, https://doi.org/10.1016/j.mset.2018.11.002.
[52] S. Zhao, Z. Wang, Z. Qiao, X. Wei, C. Zhang, J. Wang, S. Wang, Gas separation membrane with CO 2-facilitated transport highway constructed from amino carrier containing nanorods and macromolecules, J. Mater. Chem. 1 (2) (2013) 246–249, https://doi.org/10.1039/C2TA00247G.
[53] G. Liu, W. Jin, N. Xu, Graphene-based membranes, Chem. Soc. Rev. 44 (15) (2015) 5016–5030, https://doi.org/10.1039/c4cs00423j.
[54] S. Janakiram, X. Yu, L. Ansaloni, Z. Dai, L. Deng, Manipulation of fibril surfaces in nanocellulose-based facilitated transport membranes for enhanced CO2 capture, ACS Appl. Mater. Interfaces 11 (36) (2019) 33302–33313, https://doi.org/10.1021/acsami.9b09920.
[55] M. Yoo, M. Kim, Y. Hwang, J. Kim, Fabrication of highly selective PVA-g-GO/SPVA membranes via cross-linking method for direct methanol fuel cells, Ionics 20 (6) (2014) 875–886, https://doi.org/10.1007/s11581-013-1026-7.
[56] M. Mulder, J. Mulder, Basic Principles of Membrane Technology, second ed., Springer science & business media, 1996.
[57] V.E. Andreassen, Carbon Dioxide Absorption with Non-porous Hollow Fiber Membrane Contactors-Module Fabrication and Characterisation, NTNU, 2018.
[58] A.W. Adamson, A.P. Gast, Physical Chemistry of Surfaces, sixth ed. ed., Interscience publishers, New York, 1967.
[59] H. Matsuyama, M. Teramoto, K. Matsui, Y. Kitamura, Preparation of poly(acrylic acid)/poly(vinyl alcohol) membrane for the facilitated transport of CO2, J. Appl. Polym. Sci. 81 (4) (2001) 936–942, https://doi.org/10.1002/app.1514.
[60] H. Matsuyama, K. Matsui, Y. Kitamura, T. Maki, M. Teramoto, Effects of membrane thickness and membrane preparation condition on facilitated transport of CO2 through ionomer membrane, Separ. Purif. Technol. 17 (3) (1999) 235–241, https://doi.org/10.1016/S1383-5866(99)00047-7.
[61] H.Q. Lin, E. Van Wagner, B.D. Freeman, L.G. Toy, R.P. Gupta, Plasticization-enhanced hydrogen purification using polymeric membranes, Science 311 (5761) (2006) 639–642, https://doi.org/10.1126/science.1118079.
[62] R. Littel, G. Versteeg, W.P.M. Van Swaaij, Kinetics of CO2 with primary and secondary amines in aqueous solutions—II. Influence of temperature on zwitterion formation and deprotonation rates, Chem. Eng. Sci. 47 (8) (1992) 2037–2045.
[63] P.D. Vaidya, E.Y. Kenig, CO2-alkanolamine reaction kinetics: a review of recent studies, Chem. Eng. Technol. 30 (11) (2007) 1467–1474, https://doi.org/10.1002/ceat.200700268.
[64] T.L. Donaldson, Y.N. Nguyen, Carbon-Dioxide reaction-kinetics and transport in aqueous amine membranes, Ind. Eng. Chem. Fundam. 19 (3) (1980) 260–266, https://doi.org/10.1021/i160075a005.